Characterization of the Periplasmic Heme-Binding Protein ShuT from the Heme Uptake System of *Shigella dysenteriae*†

Suntara Eakanunkul,‡ Gudrun S. Lukat-Rodgers,§ Suganya Sumithran,# Arundhati Ghosh,‡ Kenton R. Rodgers,§ John H. Dawson,# and Angela Wilks*,‡

Department of Pharmaceutical Sciences, School of Pharmacy, 20 Penn Street, University of Maryland, Baltimore, Maryland 21201, Department of Chemistry, Biochemistry, and Molecular Biology, North Dakota State University, 1231 Albrecht Avenue, Fargo, North Dakota 58105-5516, and Department of Chemistry & Biochemistry, and the School of Medicine, University of South Carolina, Columbia, South Carolina 29208

Received March 4, 2005; Revised Manuscript Received July 13, 2005

ABSTRACT: The heme uptake systems by which bacterial pathogens acquire and utilize heme have recently been described. Such systems may utilize heme directly from the host's hemeproteins or via a hemophore that sequesters and transports heme to an outer membrane receptor and subsequently to the translocating proteins by which heme is further transported into the cell. However, little is known of the heme binding and release mechanisms that facilitate the uptake of heme into the pathogenic organism. As a first step toward elucidating the molecular level events that drive heme binding and release, we have undertaken a spectroscopic and mutational study of the first purified periplasmic heme-binding protein (PBP), ShuT from *Shigella dysenteriae*. On the basis of sequence identity, the ShuT protein is most closely related to the class of PBPs typified by the vitamin B_{12} (BtuF) and iron-hydroxamate (FhuD) PBPs and is a monomeric protein having a molecular mass of 28.5 kDa following proteolytic processing of the periplasmic signaling peptide. ShuT binds one *b*-type heme per monomer with high affinity and bears no significant homology with other known heme proteins. The resonance Raman, MCD, and UV−visible spectra of WT heme-ShuT are consistent with a five-coordinate high spin heme having an anionic O-bound proximal ligand. Site-directed ShuT mutants of the absolutely conserved Tyr residues, Tyr-94 (Y94A) and Tyr-228 (Y228F), which are found in all putative periplasmic heme-binding proteins, were subjected to UV−visible, resonance Raman, and MCD spectroscopic investigations of heme coordination environment and rates of heme release. The results of these experiments confirmed Tyr-94 as the only axial heme ligand and Tyr-228 as making a significant contribution to the stability of heme-loaded ShuT, albeit without directly interacting with the heme iron.

The uptake of heme as an iron source is a common mechanism by which pathogenic bacteria obtain the iron necessary for their survival and ability to establish an infection (*1*−*4*). In *Shigella dysenteriae* the heme transport genes are located within a defined genetic locus (*5*). On the basis of their sequence homology to the more well characterized siderophore based iron-uptake systems (*6*−*9*), the functions of most of the genes have been proposed (*10*). As with the uptake of iron, heme acquisition is initiated by a TonB-dependent cell surface receptor (ShuA) (*10*). Heme transport across the periplasmic space and into the cytoplasm is affected by an active transport system comprising a soluble periplasmic binding protein, a cytoplasmic permease, and an ATPase. The periplasmic binding protein ShuT bears low sequence identity to previously characterized periplasmic iron-binding proteins and includes an N-terminal region similar to that of the well characterized enterobactin-binding FepB (*11*, *12*) iron-hydroxamate binding FhuD (*13*, *14*), and vitamin B_{12}-binding BtuF proteins (*15*). Active transport across the cytoplasmic membrane is accomplished by the ShuU and ShuV proteins. On the basis of their high sequence homologies with other transport proteins such as those of the enterobactin system, ShuU and ShuV most likely comprise the cytoplasmic permease and ATPase, respectively, of a periplasmic ABC transporter[1] system (*15*−*18*). The ABC transporters are a ubiquitous family of proteins comprising two membrane spanning transporter domains and the corresponding cytoplasmic domains that, through ATP hydrolysis, drive uptake of the substrate (*19*).

Specifically, the high-affinity PBPs are critical in maintaining the selectivity and specificity of transport (*15*). The PBPs play two important roles in active transport of substrates. First, they determine the specificity of the

† This work was supported by NIH Grants AI-48551 (A.W.) and GM-26730 (J.H.D.), NCRR P20 RR15556 (K.R.R.) and USDA ND05299 (K.R.R.).

* To whom correspondence should be addressed. Tel.: 410 706-2537; fax. 410 706-5017; e-mail: awilks@rx.umaryland.edu.

‡ University of Maryland.

§ North Dakota State University.

University of South Carolina.

[1] Abbreviations: PBP, periplasmic binding protein; IPTG, isopropyl-1-thiogalactopyranoside; ABC transporter, ATP binding cassette transporter; SDS−PAGE, sodium dodecyl sulfate−polyacrylamide gel electrophoresis; IEF, isoelectric focusing; rR, resonance Raman; MCD, magnetic circular dichroism; WT, wild type; 5C HS, five-coordinate high spin; 6C HS, six-coordinate high spin.

10.1021/bi050422r CCC: $30.25
Published on Web 09/03/2005

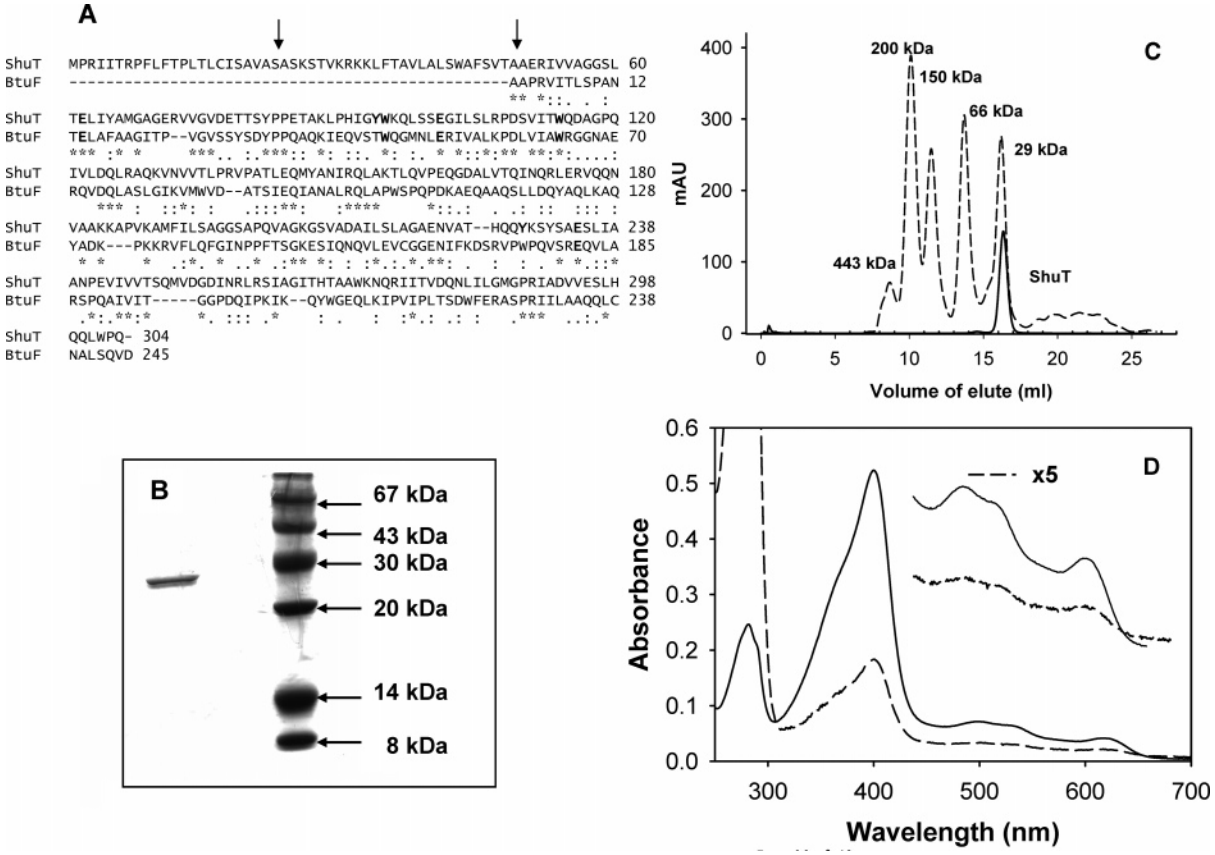

FIGURE 1: Purification and spectral properties of the heme−ShuT complex. (A) Amino acid sequence alignment of ShuT and *E. coli* BtuF. The putative signal cleavage sites are indicated by the arrows. The conserved tyrosines in all heme binding PBPs are shown in bold. The BtuF active site tryptophans and conserved glutamate residues shown to interact with the ABC transporter are also shown in bold type. (B) SDS−PAGE analysis of the purified ShuT. Molecular weight markers are as shown. (C) FPLC of the purified ShuT protein. Representative traces of the molecular weight markers are shown by the dashed line and the ShuT monomer is shown by the bold line. (D) Absorption spectra of the purified ShuT. Protein as isolated from the final ion-exchange step (dashed line). Heme−ShuT complex following addition of exogenous heme and purification over gel filtration (solid line).

transport process; second, they play an integral part in the transport process by complexing to the ABC proteins to trigger release of their substrate. The majority of the structurally characterized PBPs consist of two globular domains linked by a flexible hinge with the ligand-binding domain being defined by the interfacial cleft between the two domains. These proteins are subdivided into group I and II based upon whether they have three or two interdomain connections, respectively (*20*). More recently, a third class of PBPs has been identified typified by the vitamin B_{12} binding protein BtuF (*15*, *21*) and the iron-hydroxamate binding protein FhuD (*15*) from *Escherichia coli*. The domains of these PBPs are bridged by a single α-helical segment. The release of substrate from the PBP to the ABC transporter is thought to be coupled to the conformational changes in the periplasmic protein (*19*, *22*−*24*). Sequence homology suggests that the ShuT protein is more closely related to the recently characterized vitamin B_{12} (BtuF) and iron-hydroxamate (FhuD) periplasmic binding proteins in which the two domains are linked by an α-helical segment (Figure 1A). Although the ligand specificity of BtuF and ShuT differ, some key aromatic residues known to be directly involved in ligand stabilization are conserved as well as the critical Glu residues involved in docking to the ABC transporter (Figure 1A).

Although a number of periplasmic proteins have been purified and structurally characterized, no information on the ligation and coordination state of the heme-binding periplasmic proteins has been reported. Herein we report the first purification and characterization of the periplasmic heme binding protein, ShuT, from *S. dysenteriae*. As purified, a significant fraction (10−20%) of the protein is heme loaded. Titration with heme results in an endpoint loading of one heme per protein monomer. The heme−ShuT complex contains a five-coordinate high spin heme that is linked to the protein through a proximal Fe^{III}−O bond to the phenolate side chain of Tyr-94. The role of the ligation and binding interactions with the protein is discussed in terms of the role in sequestering and delivering heme to the cytoplasmic ABC transporter.

EXPERIMENTAL PROCEDURES

General Methods. Plasmid purification, subcloning, and bacterial transformations were carried out as previously described (*25*). Deionized, doubly distilled water was used for all experiments. Oligonucleotides were obtained from Sigma-Genosys and used without further purification. All absorption spectra of the WT and mutant heme−ShuT complexes were recorded on a Varian Carey 100Bio UV spectrophotometer. N-Terminal sequencing and mass spectroscopic analysis of the purified mature protein was performed at the Protein and Nucleic Acid Facility, The Beckman Centre, Stanford University, Palo Alto, CA.

Bacterial Strains. E. coli strain DH 5α [F′, *ara* D(*lac-proAB*) rpsL ø80d*lacZ*DM15 *hsd* R17] was used for DNA manipulation and *E. coli* strain BL21 (DE3) *pLysS* [F^- *ompT* $hsdS_B$ ($r_B^-m_B^-$) *gal dcm* (DE3)] was used for expression of both the WT and mutant ShuT constructs. Manipulation of plasmid DNA following mutagenesis was carried out in *E. coli* XL10 Gold Ultracompetent cells [Tet^r Δ*(mcrA)183* Δ*(mcrCB-hsdSMR-mrr)173 endA1 supE44 thi-1 recA1 gyrA96 relA1 lac* Hte [F′ *proAB lacI*^{q}ZΔ*M15 Tn10* (Tet^r) Amy Cam^r].

Construction of the Expression Vectors pETShuT. The ShuT gene was amplified by PCR from plasmid pSHU262 (*3*). The final gene construct encoded ShuT minus the first 22 amino acid residues of a putative signal peptide sequence (Figure 1). Primers were designed to encode within the gene an *MscI* site preceding amino acid residue 22 of ShuT in the forward primer (ShuTF) 5′-GGCCTGTGGCCATGTCTGCCTCGAAGAG-3′ and a *XhoI* site in the reverse primer (ShuTR) 5′-CTGGCTCTCGAGTTGCGGCCAAAGCTGCTG-3′. In addition, the stop codon of the *shuT* gene was removed so as to utilize the ×6-His tag preceding the *XhoI* site in the pET22b vector. The truncated *shuT* gene was subsequently cloned into pET22b utilizing the *MscI* and *XhoI* sites to generate a construct encoding the *E. coli pelB* signal peptide sequence and the truncated ShuT protein in frame with a ×6His tag.

Site-Directed Mutagenesis of ShuT. Mutagenesis was carried out utilizing the polymerase chain reaction and the Quickchange Mutagenesis kit from Stratagene (La Jolla, CA). Oligonucleotides were designed to have melting temperatures (T_m) between 65 and 75 °C. All mutations were verified by DNA sequencing of the gene construct. DNA sequencing was carried out at the Biopolymer Laboratory, School of Medicine, University of Maryland, Baltimore.

Expression and Purification of the ShuT WT and (Y94A), (Y228F), and (Y94A/Y228F) Mutant Proteins. The WT and mutant ShuT proteins were purified as follows. An overnight 10 mL inoculum in Luria Bertani (LB)-ampicillin (100 μg/mL) was prepared from LB-Amp (100 μg/mL) agar plates with freshly transformed colonies of pETShuT, pETShuT Y228A, or pETShuT Y94A in *E. coli* BL21 (DE3) *pLysS* cells. One-liter cultures were inoculated to an OD_{600} of 0.06 from a 100-mL subculture (OD_{600} = 0.6). The cells were grown to an OD_{600} of 0.6−0.8 and induced with 1 mM isopropyl-1-thiogalactopyranoside (IPTG). The cells were grown for an additional 4 h at 30 °C and harvested by centrifugation for 20 min at 6000*g* in a Beckman JA-20 rotor. The cells were gently lysed at 4 °C by stirring in 50 mM sodium phosphate (pH 8.0) containing 100 mg of lysozyme/100 mL of cell lysate, 0.2 mM PMSF and 1 protease inhibitor cocktail tablet (Roche Diagnostics GmbH).

The periplasmic fraction was obtained by centrifugation at 3000*g* for 30 min in a Beckman JA-20 rotor. The resulting supernatant was then centrifuged for an additional 30 min at 6800*g*, and the clarified solution was applied to a Ni−NTA agarose column (1 × 10 cm) previously equilibrated in 20 mM Tris-HCl (pH 7.8) containing 5 mM imidazole and 300 mM NaCl. The column was washed with 10 column volumes of the same buffer followed by the same buffer containing 20 mM imidazole. The protein was eluted in 20 mM Tris-HCl (pH 7.8) containing 250 mM imidazole and 300 mM NaCl. The peak fractions as judged by SDS−PAGE were pooled and dialyzed against 20 mM Tris-HCl (pH 7.5). Following dialysis, the protein was concentrated to 10 mg/mL and stored at −80 °C. Fully heme-loaded ShuT was prepared by titrating the protein with a freshly prepared solution of 10 mM hemin in DMSO to a heme-to-protein ratio of 2:1. Excess heme was removed by passage over a Sephacryl S-100 column (1 × 100 cm) previously equilibrated in 20 mM Tris-HCl (pH 7.5). The resulting holoprotein was concentrated and stored as described above. Protein concentrations were determined on the basis of absorbance at 280 nm using ϵ_{280} = 30.71 mM^{-1} cm^{-1}. The value of ϵ_{280} for the native protein was determined as follows: The absorbance at 280 nm of the native protein, AN_{280}, was measured for ShuT. The protein was then denatured in 6.0 M guanidinium hydrochloride at pH 6.5, 0.2 M potassium phosphate. Absorbance at 280 nm of the denatured protein, AD_{280}, was again measured and the protein concentration was determined using the empirically calculated extinction coefficient of ϵ_{D280} = 30.4 mM^{-1} cm^{-1} (http://www.expasy.org). The extinction coefficient (ϵ_{N280}) for the native protein was then calculated from A_{280} of the folded (AN_{280}) and denatured (AD_{280}) proteins (accounting for dilution with denaturant), and ϵ_{280} according to eq 1.

$$\epsilon_{N280} = \epsilon_{D280}(AN_{280}/AD_{280}) \quad (1)$$

The isoelectric point (pI) of the purified mature protein was determined by isoelectric focusing (IEF) on an Amersham Pharmacia PHAST system. ShuT (3 μg) was loaded onto the Phastgel IEF range 3−9 along with protein markers in the range 4.45−9.6. Following a prefocusing step, the proteins were run at 15 °C, 2.5 mA, and 75 V for 1 h. The gel was fixed for 10 min in 20% (w/v) trichloroacetic acid for 2 min and washed in a 1:1 mixture of solution A (0.2%-(w/v) $CuSO_4$ + 20% acetic acid) and B (60% (v/v) methanol). The gel was then stained for 15 min using in a 1:1 mixture of solutions A and C (0.4 g of Coomasie blue in 400 mL of water). Destaining was performed for 15−20 min using a 1:1 mixture of solutions A and B. The gel was further fixed in 5% glycerol and 10% acetic acid for 10 min followed by air-drying overnight.

Size-Exclusion Chromatography. The native molecular mass of ShuT was analyzed on a Pharmacia AKTA FPLC system fitted with a Superdex S200 HR 10/30 column equilibrated in 20 mM Tris (pH 8.0) containing 100 mM NaCl. A 50 μL sample at a final concentration of 100 μM of either the apo- or holoprotein was injected onto the column and the elution volume noted. In a separate experiment, the molecular weight markers (50 μL) were injected to obtain a standard curve across the range 669 kDa to 17 kDa.

UV−Visible Absorbance Spectroscopy. The electronic absorbance spectra of the heme−ShuT complexes were recorded in 20 mM Tris (pH 7.5) on a Cary 100Bio spectrophotometer. The extinction coefficients (ϵ_{400}) for the heme−ShuT complexes were determined as previously described (*3*). The absorbance spectrum of a purified heme−ShuT sample was taken and an excess of dithionite added after which the spectrum of the pyridine hemochrome was recorded. The heme concentration was calculated from the absorbance maxima at 418.5, 526, and 555 nm using extinction coefficients of 170, 17.5, and 34.4 mM^{-1} cm^{-1}, respectively. For heme−ShuT, ϵ_{400} was calculated assuming

a heme/ShuT ratio of 1:1 as determined by titration of apo-ShuT with heme. Heme content in apo-ShuT was calculated using the pyridine hemochrome method outlined above. UV−visible spectra of the heme−ShuT complexes were recorded in 20 mM Tris-HCl between pH 5 and 10.

Heme-Binding Studies. Heme binding was tracked by difference (ΔAbsorbance) spectroscopy in the Soret region of the UV−visible spectrum at 25 °C. Successive aliquots of 1 mM hemin in DMSO were added to both the sample cuvette, which contained 10 μM apo-ShuT, and reference cuvette. Spectra were recorded 10 min after the addition of each heme aliquot.

Heme binding was also monitored by fluorescence quenching measurements of the tryptophan residue in the mature native ShuT. Fluorescence intensities at 337 nm were recorded at 25 °C in 20 mM Tris-HCl (pH 7.8) with a ShuT concentration of 10 μM using a Perkin-Elmer LS-50 luminescence spectrometer with excitation set at 295 nm. Heme was added to the buffered protein solutions in 1.0 μL aliquots, and the titrations covered a heme concentration range of 0.1−50 μM. Solutions of heme in DMSO were used within 30 min of being made. The dissociation constant (K_d) was calculated by Scatchard analysis from the decrease in fluorescence at 337 nm as a function of increasing heme concentration.

Heme Dissociation from WT ShuT, ShuT (Y94A), (Y228F), and (Y94A/Y228F) Mutants. Heme dissociation reactions for the WT ShuT were carried out in a 1 mL reaction volume containing 10 μM heme−ShuT and 50 μM apo-myoglobin in 20 mM Tris-HCl (pH 8.0) at 25 °C. Reactions were initiated by addition of apomyoglobin to a solution of the heme−ShuT complex and full UV−visible absorbance spectra were recorded between 300 and 700 nm at 60-s intervals. Single-wavelength absorbance versus time curves were also recorded at 407 nm. The initial rates of heme transfer to apomyoglobin were measured for the WT ShuT protein. The rate of heme transfer from the Tyr mutants was significantly faster than that for the WT ShuT and were measured by stopped-flow spectrometric methods on an Applied Photophysics instrument with a diode-array detector. Spectra were recorded over the range 350−700 nm at given time intervals over the course of the reaction. The reactions were carried out with heme-Y94A, heme-Y228F, or heme-Y94A/Y228F ShuT (10 μM) in syringe A and apo-myoglobin (50 μM) in 20 mM Tris-HCl (pH 7.8) in syringe B. After the samples were mixed, spectra were recorded between 350 and 700 nm at fixed intervals until no further changes occurred. In addition, kinetic time courses at the desired individual wavelengths were also recorded. All spectra were collected at 22 °C. Kinetic data analysis was performed assuming first-order reaction kinetics. Data were fit using a global analysis algorithm kinetic program Pro-Kineticist provided by Applied Photophysics.

Resonance Raman Spectroscopy. Resonance Raman (rR) spectra were obtained from 30 to 70 μM ShuT samples housed in a 5-mm NMR tube spinning at ∼20 Hz. Raman spectra were recorded using either 406.7 nm emission from a Kr^+ laser (10−25 mW) or 514.5 nm emission from an Ar^+ laser (85−120 mW). UV−visible absorbance spectra were recorded before and after the rR experiments to ensure that the samples were not irreversibly altered in the laser beam. No spectral artifacts attributable to laser-induced sample damage were observed. Spectra were recorded at ambient temperature using 135° backscattering geometry with the laser beam focused to a line. Scattered light was collected with an f1 lens and filtered with a holographic notch filter to attenuate Rayleigh scattering. The polarization of the scattered light was then scrambled, and the spot image was f-matched to a 0.63-m spectrograph fitted with a 2400 groove/mm grating and a LN_2 cooled CCD camera. The spectrometer was calibrated using the Raman bands of toluene and DMF as external frequency standards.

Magnetic Circular Dichroism Spectroscopy. Magnetic circular dichroism (MCD) spectra were recorded at 4 °C and 1.41 T on a Jasco J600 spectropolarimeter fitted with a Jasco MCD-1B electromagnet. Data acquisition and manipulation were done as previously reported with JASCO software (*26*). UV−visible absorbance spectra were recorded before and after MCD measurements to check the sample integrity. All spectra were obtained using quartz cuvettes with either 0.5 or 1 cm path lengths. All ShuT protein samples were examined in 20 mM Tris (pH 7.5). The imidazole adduct of ferric heme-ShuT(Y94A/Y228F) was prepared by microliter titration with 1 M imidazole stock solution until no further changes were observed in the absorbance spectrum. The sample of ferric H93G (phenolate/water) myoglobin was prepared as previously described (*27*) except for the use of phenol (final concentration, 50 μM) as the added ligand.

EPR Spectroscopy. X-band EPR spectra were recorded with a commercial spectrometer fitted with a liquid He cryostat. The samples were ∼300 μM in heme and were buffered at pH 7.5 in 100 mM Tris. Spectra were recorded at 5 K with 10 G field modulation at 100 kHz. Scan speed and signal time constant were always set such that their product was less than the field modulation amplitude.

RESULTS

Expression and Purification of ShuT. Prior analysis of the full-length sequence of ShuT utilizing the SignalP program (http://www.expasy.org) (*28*) indicated two possible signal peptide cleavage sites within the first 49 amino acids of the full-length ShuT gene (Figure 1A). The mature soluble ShuT protein was secreted to the periplasm as judged by SDS−PAGE of the periplasmic fraction (data not shown). Following purification over a Ni−NTA agarose column, the protein gave a single band of molecular mass 28.5 kDa based on SDS−PAGE analysis (Figure 1B) and size-exclusion chromatography (Figure 1C). Subsequent analysis of the purified protein by electrospray mass spectrometry yielded a molecular mass of 28.3 kDa, consistent with cleavage at the second signal peptide site, which was further confirmed with the sequence AERIVVAGGS obtained on N-terminal sequence analysis.

Guided by rR signatures characteristic of heme proteins having a proximal tyrosinate ligand (vide infra), a sequence alignment of ShuT with other periplasmic binding proteins (PBPs) was undertaken. The first striking feature of this alignment was the lack of a conserved histidine. This together with the resistance toward dithionite reduction, as seen for HbM's Iwate, Boston, and Hyde Park (*29*) and the lack of MCD signatures for an axial His ligand eliminated the likelihood of a Tyr−His ligated heme as is found in HasA. However, the sequence alignment did reveal two completely

Table 1: UV−Visible Absorbance Characteristics of Heme−ShuT and Its Tyr Mutants

ShuT construct	Soret max (nm)	visible max (nm)	K_d (μM)	apparent rate constant for transfer of heme to apo-Mb (s^{-1})	ϵ_{400} (mM^{-1} cm^{-1})
WT	400	500, 521, 617	nd[a]	4×10^{-5}	102.70
Y94A	399	600	26	0.59	83.02
Y228F	401	500, 521, 600	11.7	0.0174	91.92
Y94A/Y228F	396		52.2	0.16	73.99

[a] Not determined due to the ShuT protein containing residual heme on purification.

conserved tyrosines corresponding to Y94 and Y228 in ShuT. Efforts thereafter were focused on carrying out site-directed mutagenesis of these residues to determine whether one or more of the conserved Tyr side chains coordinate to the heme. Like the WT protein, the mutants were efficiently secreted to the periplasm and had molecular weights consistent with that of WT ShuT. The mature ShuT protein when expressed and purified from *E. coli* cells was 10−20% loaded with heme (Figure 1D). In contrast to the WT protein the Y228F, Y94A and Y228F/Y94A ShuT mutants were isolated without detectable heme (data not shown).

UV−Visible Absorbance Spectra of the Heme-Loaded WT ShuT and Its Tyr Mutants. The Soret maximum of the heme−ShuT complex after loading with heme occurs at 400 nm with visible bands at 500, 521, and 617 nm (Figure 1D and Table 1). In contrast to the WT ShuT, heme complexes of the Y94A, Y228F, and Y94A/Y228F mutants have diminished stabilities. As will be shown below, their stabilities are on the order of 10^3 lower than the WT protein. UV−visible spectra of the heme-loaded Y94A and Y94A/Y228F mutants were distinct from that of WT heme−ShuT. By contrast, the spectrum heme−ShuT (Y228F) was almost identical to that of its WT counterpart.

The spectrum of heme ShuT (Y94A) exhibits a Soret maximum at 399 nm, loss of the 500 and 521 nm bands, and a much diminished band in the 600 nm region (Table 1). The spectra of heme−ShuT(Y228F) and heme−ShuT-(Y94A/Y228F) are similar to those of WT heme−ShuT and heme−ShuT(Y94A), respectively (Table 1). The millimolar extinction coefficients at 400 nm (ϵ_{400}) calculated by the pyridine hemochrome method are also shown in Table 1.

Interestingly, the absorbance spectra of WT heme−ShuT and heme−ShuT (Y228F) are insensitive to pH over the range of 5−10, strongly suggesting that the coordination number, axial ligand identities, and spin state of the Fe(III) center are similarly pH independent. In contrast, we were unable to measure the pH dependence of the ShuT (Y94A) and (Y94A/Y228F) heme complexes due to their instabilities below pH 6 and above pH 8.5. Coordination number, axial ligand identity, and spin-state of heme-ShuT and the heme-ShuT mutants will be further discussed in the following sections.

Spectrophotometric titration of WT apoShuT with a DMSO solution of hemin showed saturation at a heme/ShuT ratio of 1:1. This value takes into account the fraction of heme-loaded ShuT after isolation and purification. Similarly, titration of the ShuT (Y94A), (Y228F), and (Y94A/Y228F) mutants with hemin showed a loading stoichiometry of 1:1 (data not shown). Resistance of the isolated WT ShuT to complete removal of heme precluded accurate determination of K_d. Attempts to remove the heme by cold acid−acetone extraction followed by refolding of the protein proved unsuccessful. Given that the Tyr mutants investigated in this study are isolated without detectable loading of heme, it is reasonable to conclude that their affinities for heme are lower than WT ShuT. The dissociation constants for the Tyr mutants, as determined by absorbance and/or fluorescence methods, are in the tens of micromolar range. In an effort to gain some insight into the affinity of WT ShuT for heme, we exploited the ability of apomyoglobin ($K_d = 10^{-14}$ M) to extract the heme from the holo-ShuT in a reaction whose rate is likely limited by dissociation of heme from holoShuT. Addition of a 5:1 molar excess of apomyoglobin to the heme−ShuT complex at pH 7.4 results in extraction of heme from the ShuT, as judged by the shift in the Soret band maximum from 400 to 407 nm. This reaction was complete in approximately 1 h (Figure 2B). In contrast, heme extraction from heme−ShuT (Y94A), (Y228F), and (Y94A/Y228F) were complete within one minute (Figure 2C). Kinetic analysis of these reactions based on ΔA_{407} as a function of time revealed that they are first order in heme−ShuT (Table 1). As would be expected based on the results outlined in the following section, the approximate 10^4 increase in dissociation rate of heme−ShuT (Y94A) and (Y94A/Y228F) mutants is indicative of loss of the proximal ligand. Additionally, the increase in dissociation rate from heme−ShuT (Y228F) over that of the WT protein accounts for a corresponding increase of approximately 10^2 in K_d. Since a reliable rate constant for the binding of heme by apoShuT has not been determined, the affects of the Tyr-228 mutation on k_{assoc} and its contribution to the stability of holoShuT remains unclear.

Heme Spin State and Axial Ligand Identification from Resonance Raman Spectroscopy of Ferric WT ShuT and Its (Y228F), (Y94A), and (Y94A/Y228F) Mutants. Oxidation state, spin state, and coordination state marker bands for heme proteins are observed in the high-frequency region of their rR spectra. The high-frequency Soret-excited spectra for WT ShuT and the three mutants are shown in Figure 3. The υ_4 band, characteristic of porphyrin π^* electron density and iron oxidation state, occurs near 1370 cm^{-1} for all four of the ShuTs and is indicative of ferric heme. For WT ShuT, the spin-state marker band, ν_3 is observed at 1484 cm^{-1} consistent with a high spin heme. Resonance Raman scattering by the modes giving rise to the marker bands ν_{10} and ν_{19} are well enhanced with Q-band excitation and are assigned at 1616 and 1566 cm^{-1}, respectively, in the 514.5-nm excited rR spectrum of WT ShuT shown in Figure 4. The ν_3 (1487−1494 cm^{-1}, 5c HS; 1478−1482 cm^{-1}, 6c HS), ν_{10} (1622−1626 cm^{-1}, 5c HS; 1605−1612 cm^{-1}, 6c HS), and ν_{19} (1565−1576 cm^{-1}, 5c HS; 1548−1562 cm^{-1}, 6c HS) frequencies are also sensitive to the heme coordination number. Although the ν_3 frequency for WT ShuT is at the low end of the frequency range for a 5C HS, it is consistent with those reported for 5c HS hemoproteins having a proximal tyrosine ligand, i.e., heme catalases (*30*, *31*). The ν_3, ν_{10}, and ν_{19} frequencies observed for WT ShuT and the Tyr mutants are similar and are typical of 5c HS ferric

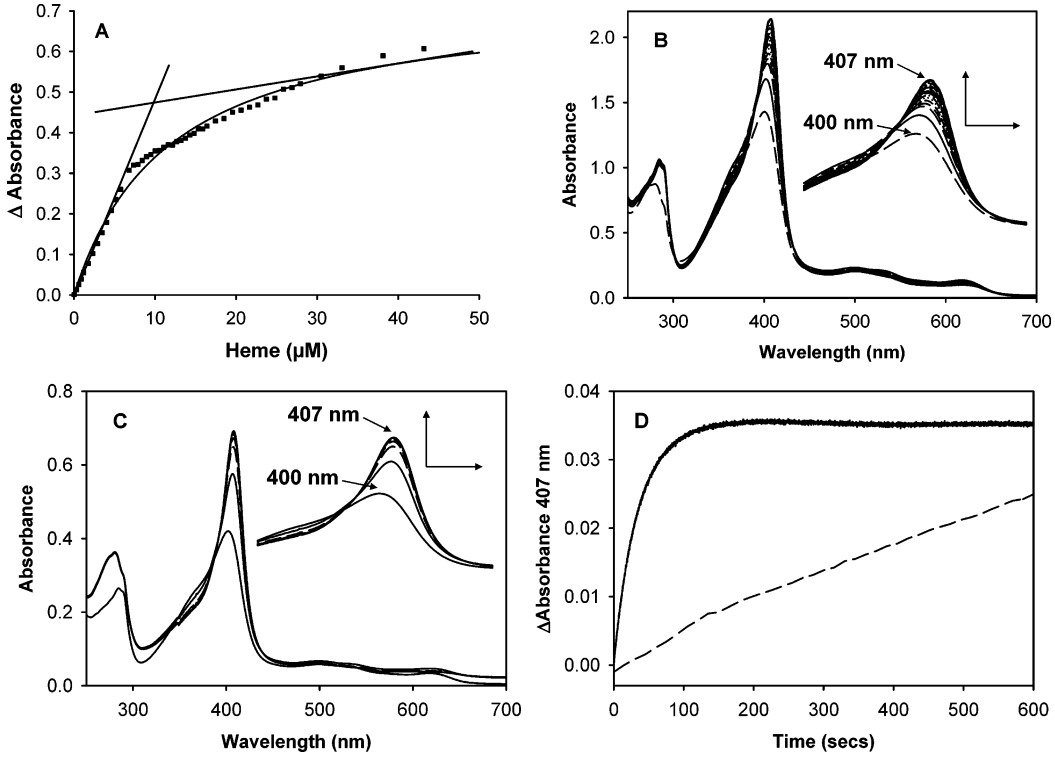

FIGURE 2: Heme binding and displacement from the ShuT and Y228F mutant complexes. (A) Difference absorption spectroscopy measured as the difference at 400 nm following incremental addition of heme (0.1−50 μM) to ShuT (10 μM) in 20 mM Tris (pH 7.8) against a blank containing buffer alone. (B) Heme displacement from ShuT (10 μM) by apo-myoglobin (50 μM) in 20 mM Tris (pH 7.8) spectra measured at 1-min intervals over a period of 60 min. (C) Heme displacement from the Y228F ShuT mutant as described above except spectra were recorded at 0.1 min intervals. (D) Time courses for hemin displacement from the heme-ShuT (dashed line) and Y228F ShuT (solid line). Reactions were carried out as described above, and the rate of transfer of heme to apo-myoglobin was measured by the increase in absorbance at 407 nm.

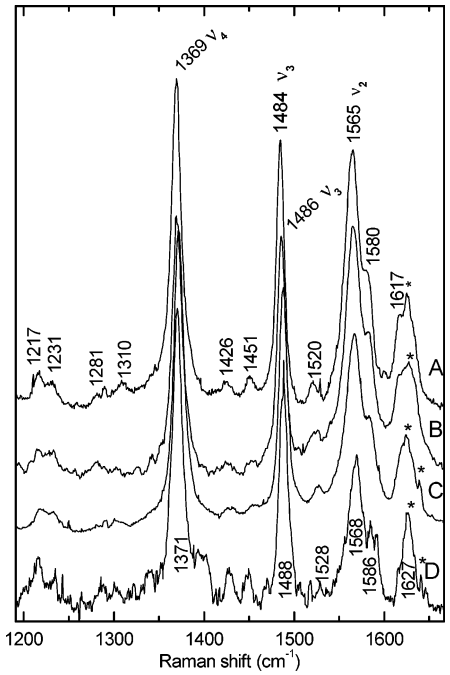

FIGURE 3: High-frequency resonance Raman spectra of ferric WT ShuT in 20 mM Tris/HCl pH 8.0 (A), ShuT(Y228F) in 20 mM Tris/HCl pH 7.8 (B), ShuT(Y94A) in 20 mM Tris/HCl pH 7.8 (C), and ShuT(Y228F/Y94A) in 20 mM Tris/HCl pH 8.0 (D) obtained with 406.7 nm excitation. Asterisk indicates plasma lines.

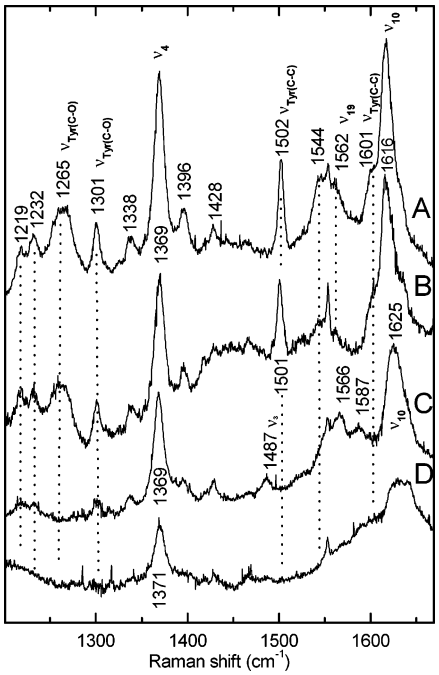

FIGURE 4: High-frequency resonance Raman spectra of ferric WT ShuT (A), ShuT(Y228F) (B), ShuT(Y94A) (C), and ShuT(Y228F/Y94A) (D) obtained with 514.5 nm excitation. Buffer conditions for the samples are the same as in Figure 3.

hemoproteins. The largest spectral difference between WT ShuT and the Tyr mutants lies in the frequencies of the spin state marker band ν_{10}. As for ν_3, the ν_{10} bands in the WT ShuT and ShuT(Y228F) spectra both occur at frequencies toward the low end of the range for five-coordinate-high spin hemes (1616 cm^{-1}). The higher frequency ν_{10} bands in the ShuT(Y94A) and (Y228F/Y94A) spectra (1625 cm^{-1}) are typical of 5c HS hemoproteins.

Table 2: Heme Vibrational Bands for Ferric Heme Proteins with Tyrosinate Heme Ligation

protein	coord no., spin state	ν_2	ν_3	ν_4	ref
Hb M Boston	5c HS	1571	1487	1367	(*29*)
Hb M Hyde Park	5c HS	1563	1486	1369	(*29*)
Hb M Iwate	5c HS	1570	1486	1368	(*29*)
Hb M Saskatoon	6c HS	1563	1476	1367	(*29*)
Chlamydomonas Hb	6c HS		1477	1370	(*57*)
Mb(H93Y)	5c HS	1572	1492	1372	(*35*, *48*)
bovine liver catalase	5c HS	1568	1484	1373	(*42*)
A. nigar catalase	5c HS	1574	1489	1373	(*31*)
M. luteus catalase	5c HS	1570	1489	1374	(*31*)
human heme oxygenase-1(H25Y)	5c HS	1570	1491	1370	(*32*)
CcmE	5c HS		1492	1373	(*36*)
WT ShuT	5c HS	1565	1484	1369	this work
ShuT Y228F	5c HS	1565	1486	1370	this work
ShuT Y94A	5c HS	1568	1488	1372	this work
ShuT Y228F/Y94A	5c HS	1568	1488	1372	this work

Table 3: Tyrosinate Vibrational Bands for Ferric Heme Proteins with Tyrosinate Ligation

proteins	resonance Raman frequencies (cm^{-1}) $\nu_{Tyr(C=C)}$	$\nu_{Tyr(C=C)}$	$\nu_{Tyr(C-O)}$	$\nu_{(Fe-O)}$	ref
Chlamydomonas Hb	NR[a]	NR	NR	502	*(57)*
Hb-M Saskatoon	1607	1504	1300	578	(*59*)
human Mb(H93Y)	1603	1504	1302	585	(*48*)
sperm whale Mb(H93Y)	NR	1506	1303	586	(*35*)
Hb M Iwate	1607	1504	1308	588	(*58*, *59*)
Hb M Hyde Park	1609	1502	1300	588	(*59*)
human HO-1(H25Y)	1605	1504	1258	591	(*32*)
Hb M Boston	NR	1505	1278	603	(*58*, *59*)
bovine liver catalase	1612	~1520	1244	NR	(*42*)
A. nigar catalase	1615	NR	1245	NR	(*31*)
CcmE	1605	NR	NR	600	(*36*)
WT ShuT	1601	1502	13011265	613	this work
ShuT(Y228F)	1601	1501	13011265	613	this work

[a] NR indicates not reported.

In Soret-excited spectra of hemoproteins, scattering by the ν_4 mode is typically the most resonance enhanced and gives rise to the most intense band in the spectrum. The high-frequency Soret-excited rR spectra of all four ShuT proteins are shown in Figure 3. They are unusual in that the ν_4 and ν_3 bands are almost of equal intensity. The intensity ratios I(ν_4)/I(ν_3) for WT ShuT, ShuT (Y228F), ShuT(Y94A), and ShuT(Y228F/Y94A) are 1.2, 1.1, 1.3, and 1.5, respectively. Ratios near 1.0 have also been reported for two proximal His mutants of HO, HO(H25Y) at pH 7.4 and HO (H25A) at pH 10.0 (*32*, *33*). HO(H25Y) is a 5c HS hemoprotein with a proximal tyrosinate ligand (*32*); a hydroxide ion, or the carboxylate side chain of a glutamate residue have been suggested as potential fifth ligands in 5c HS HO(H25A) (*33*, *34*). Soret-excited rR spectra of the heme-containing *Asperillus niger* catalase (*31*), Mb(H93Y) (*35*), and CcmE (*36*), three 5c HS hemoproteins having proximal tyrosinate ligands, also exhibit relatively low I(ν_4)/I(ν_3) ratios (~1.5). Finally, in alkaline solution the cavity mutant of Mb, Mb(H93G), yields a spectrum with marker band frequencies typical of 5c HS heme (*37*) and I(ν_4)/I(ν_3) = 1.5. Taken together, these data suggest that the low I(ν_4)/I(ν_3) ratio (1.5) is a spectroscopic signature of 5c HS hemes having an axial anionic ligand bound through an oxygen atom. Thus, although the electronic basis for this unique resonance enhancement pattern is not clear at present, the Soret-excited rR spectra of all four ShuT proteins exhibit it and are consistent with 5c HS RO^- ligated hemes. Table 2 compares vibrational parameters for the ShuT proteins with those of other heme-tyrosinates.

Proximal Tyrosinate Identification Based on rR Bands of Bound Phenolate. For tyrosinate ligated hemoproteins, excitation into the tyrosinate-Fe(III) CT band (near 500 nm) of tyrosinate liganded hemes yields characteristic vibrational frequencies for bound phenolate. The 514.5 nm excited rR spectra for WT ShuT and ShuT(Y228F) (Figure 4) contain these signature bands, strongly suggesting assignment of the proximal ligand as tyrosinate in these two proteins. The frequencies of the internal tyrosinate modes in WT ShuT and ShuT(Y228F) are compared with those of other heme-tyrosinates in Table 3. The ν_{Fe-OPh} modes reported to date for tyrosinate ligated hemes fall in a frequency range of 502−603 cm^{-1}. The band most likely attributable to ν_{Fe-OPh} in the spectra of WT ShuT and ShuT(Y228F) occurs at 613 cm^{-1} (Figure 5), 10 cm^{-1} higher than previously reported ν_{Fe-OPh} frequencies. Whether this difference arises because of differences in the Fe−O bond strengths or differences in Fe−O−Ph bond angles, and/or tyrosinate ring orientation relative to the heme plane is uncertain at this time.

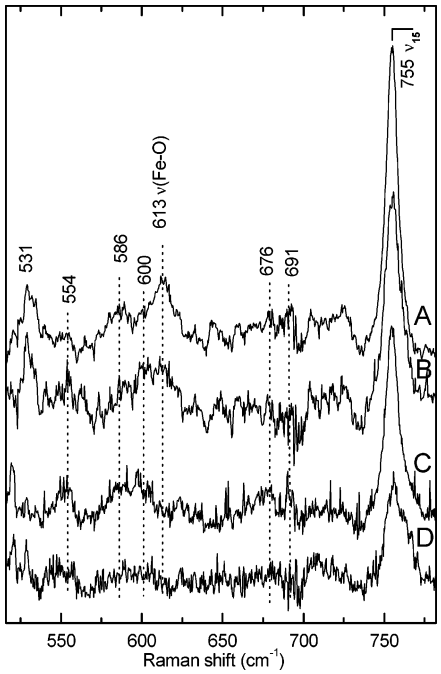

FIGURE 5: Low-frequency resonance Raman spectra of WT ShuT (A), ShuT(Y228F) (B), ShuT(Y94A) (C), and ShuT(Y228F/Y94A) (D) obtained with 514.5 nm excitation. Buffer conditions for the samples are the same as in Figure 3.

While bands attributable to ν_{Fe-OPh} and internal tyrosine vibrations are observed in the 514.5-nm excited resonance Raman spectra of WT and ShuT(Y228F), they are absent in the corresponding spectra of ShuT(Y94A) and ShuT(Y228F/Y94A) (Figures 4 and 5). Thus, although the ν_3, ν_{10}, and ν_{19} frequencies indicate that the heme remains 5c and HS and I(ν_4)/I(ν_3) is characteristic of an anionic O-bound ligand (Figure 3), the absence of bands attributable to an axial tryosinate ligand in the spectra of ShuT(Y94A) and ShuT-

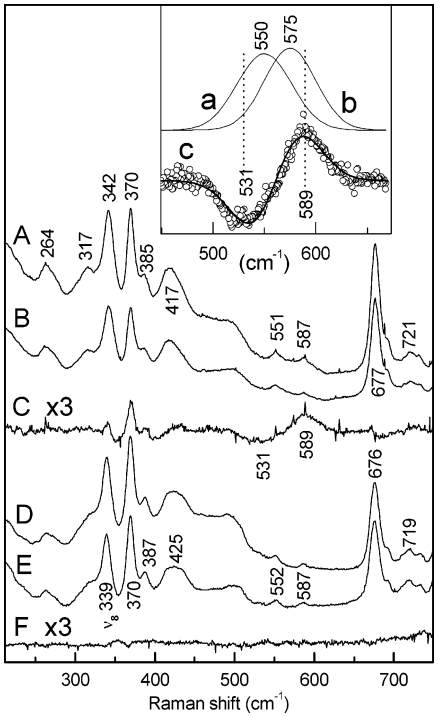

FIGURE 6: Low-frequency resonance Raman spectra of (A) ferric ShuT(Y94A) in 20 mM Tris/HCl pH 8.0, 100% $H_2{}^{16}O$, (B) ferric ShuT(Y94A) in 20 mM Tris/HCl pH 8.0, 75% $H_2{}^{18}O$, 25% $H_2{}^{16}O$, (C) spectrum A-spectrum B, (D) WT ShuT in 20 mM sodium phosphate pH 7.2, 100% $H_2{}^{16}O$, (E) WT ShuT in 20 mM sodium phosphate pH 7.2, 80% $H_2{}^{18}O$, 20% $H_2{}^{16}O$, and (F) spectrum D − spectrum E. All spectra were obtained with 406.7 nm excitation with between 10 and 15 mW of power at the sample. Inset: Simulated difference spectrum of ShuT(Y94A) ($H_2{}^{16}O-H_2{}^{18}O$). The difference spectrum was fit by setting the frequency difference between the isotopically shifted bands to the 25 cm^{-1}. The frequencies and widths of these bands were optimized to yield the best fit (solid line, c) to the experimental data (open circles, c). The maximum (589 cm^{-1}) and minimum (531 cm^{-1}) were reproduced by bands centered at 575 (b) and 550 (a) cm^{-1} and having bandwidths of 50 cm^{-1}.

(Y228F/Y94A) indicates that Tyr-94 is the missing ligand. Moreover, lack of iron-tyrosinate vibrational signatures in the spectrum of ShuT(Y94A) suggests that Tyr-228 does not coordinate to the heme when Tyr-94 is unavailable. Hence, ShuT(Y94A) and ShuT(Y94A/Y228F) contain 5c HS hemes which could have an axial hydroxide or carboxylate ligand from an Asp or Glu residue, analogous to the case of HO-(H25A) (*33*).

To address the possibility of an exogenous hydroxide ligand, the low-frequency resonance Raman spectrum of ShuT(Y94A) was examined for an Fe−OH stretching mode, which can be identified by its sensitivity to $^{18}OH^-$ substitution. The effects of this substitution are shown in Figure 6. Although significant differences are not readily observed between the parent spectra recorded in $H_2{}^{16}O$ (Figure 6A) and $H_2{}^{18}O$ (Figure 6B), an isotopically sensitive mode is easily identified in their difference spectrum (Figure 6C). The broad difference feature, with a maximum at 589 cm^{-1} and a minimum at 531 cm^{-1}, is assigned to the Fe−OH stretching mode (ν_{Fe-OH}) for 5c HS ShuT(Y94A). The apparent shift of 58 cm^{-1} is significantly larger than that calculated for an isolated harmonic Fe−OH oscillator (23.8 cm^{-1}). While the observed isotope shifts for 5c HS hydroxide complexes in proteins [e.g., Mb(H93G), 575 to 551 cm^{-1} (*37*); *Scapharca* inaequivalvis HbI, 578 to 553 cm^{-1}(*38*), HmuO(H20A), 601 to 575 cm^{-1} (*39*)] are in good agreement with this calculated shift, the 58 cm^{-1} apparent shift shown in Figure 6 is explained by a frequency separation of the isotopically shifted bands that is less than their bandwidths. The inset in Figure 6 illustrates this effect for ShuT(Y94A)-OH. The difference spectrum obtained for ShuT(Y94A) ($H_2{}^{16}O-H_2{}^{18}O$) was simulated using bandwidths of 50 cm^{-1}. The simulated spectra indicate that the ν_{Fe-OH} for ShuT-(Y94A) is ∼ 575 cm^{-1}, in good agreement with reported ν_{Fe-OH} for 5c hydroxide complexes of the aforementioned heme proteins. While the 50-cm^{-1} ν_{Fe-OH} bandwidth shown in the inset of Figure 6 is greater than the ∼20 cm^{-1} bandwidths reported for other 5c HS proteins (*37*, *38*), bandwidths of 60 and ∼65 cm^{-1} have been reported for free hemin in SDS micelles (*40*) and aqueous iron porphyrinate model complexes (*41*), respectively. The broad ν_{Fe-OH} band in the ShuT(Y94A) spectrum suggests conformational heterogeneity in the Fe−OH environment of this mutant. In the absence of Tyr-94, which normally anchors the heme to the protein, the heme must be held in place by nonbonded interactions between the heme and the protein. Under these conditions the heme environment is likely to be more dynamic than in the WT protein, thereby permitting the Fe−OH moeity to access a range of conformations.

The origin of the difference features that are observed around 340 and 370 cm^{-1} in the ShuT(Y94A) ($H_2{}^{16}O-H_2{}^{18}O$) spectrum is unclear. Similar difference features have been reported for hemin in SDS micelles and have been attributed to slight differences in intensity and in frequency of intense bands in the parent spectra rather than isotope sensitivity (*40*). Bands generally assigned to ν_8 and δ-$(C_\beta C_c C_d)_{6,7}$ (the bending modes for heme propionate groups) are intense bands observed at 342 and 370 cm^{-1}, respectively, for ShuT(Y94A). Slight differences in their intensities are seen and could be responsible for the ShuT(Y94A) ($H_2{}^{16}O-H_2{}^{18}O$) difference features. Another possibility is that these modes involve slight motion of the axial hydroxide oxygen atom, which would confer isotope sensitivity on their frequencies. The low-frequency resonance Raman spectrum of WT ShuT was also examined for isotope sensitivity in $H_2{}^{16}O$ and $H_2{}^{18}O$. Since WT ShuT contains a 5c HS heme with Tyr-94 as its proximal ligand, no $H_2{}^{18}O$-sensitive bands are expected. Spectra D, E, and their difference spectrum, F are presented in Figure 6 for comparison with the ShuT-(Y94A) spectra. They show no evidence of isotope sensitivity in the Fe−OH stretching region of the spectrum.

The rR spectrum of WT ShuT is remarkably insensitive to pH over the range from 5.2 to 11.4 with only slight broadening of the bands at pH 12, probably due to the onset of denaturation (Figure 7). Analogous insensitivity to pH has also been reported for the rR spectrum of heme catalases (*42*). This behavior is not particularly surprising given that the heme is linked to the protein through the anionic proximal ligand, tyrosinate. For the heme to take on an overall negative charge by binding an anionic hydroxide ligand would likely be unfavorable. Precedence for the difficulty in forming a bis-anion complex is found in aqueous iron-porphyrin model complexes where it has been shown that conversion of (Fe-(T(2-N-Mepy)P)(OH)(OH_2))$^{4+}$ to (Fe(2-N-Mepy)P)$(OH)_2)^{3+}$ occurs with a pK_a ∼ 11 (*41*). Given that this conversion occurs in a complex having an overall charge of 4^+ in an

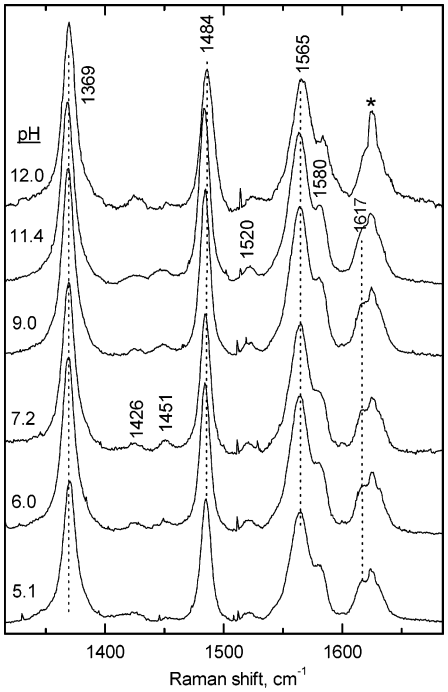

FIGURE 7: High-frequency resonance Raman of WT ShuT as a function of pH obtained with 400.7 nm excitation.

aqueous environment, it is not surprising that in a protein environment where the overall charge of the heme-tyrosinate is negative (due to the tyrosinate ligand and peripheral propionate groups), binding of another anionic axial ligand (hydroxide) would be costly and unlikely to occur within the range of pH stability of the native protein fold. Accordingly, there is currently no example of a ferric heme protein comprising two anionic O-bound axial ligands.

Magnetic Circular Dichroism Spectroscopy of heme−ShuT and ShuT (Y94A), (Y228F), (Y94A/Y228F) Mutants. Magnetic circular dichroism (MCD) spectroscopic signatures of heme proteins are well correlated with the various axial ligands and ligand field strengths. As such, the MCD signatures provide a basis for identifying axial ligands and spin states in uncharacterized heme environments. This is accomplished by examining the MCD spectra of the uncharacterized heme and exogenous ligand adducts, followed by comparison of the resulting spectra with those of structurally characterized heme proteins and/or iron-porphyrin model complexes (*27*).

The MCD spectra of ferric WT ShuT and of the ferric myoglobin heme cavity mutant Mb(H93G) in the presence of phenol are compared in Figure 8A. These spectra exhibit similar features, albeit with slight differences in intensity. Further characterization by stoichiometric titration of Mb(H93G) with phenol indicates that the resulting phenolate complex is five-coordinate high spin (Perera, R. and Dawson, J.H, unpublished data). Therefore, on the basis of the MCD and the rR data outlined above, we can conclude that the WT heme−ShuT complex is five coordinate with an anionic O-bound axial ligand. Figures 8 and 9 compare the MCD spectra of ferric ShuTs having different sets of axial ligands due to mutation of the two conserved Tyr residues. As shown in Figure 8B, the spectrum of ferric ShuT(Y94A) is significantly different from that of the wild-type ferric ShuT, while that of ferric ShuT(Y228F) (Figure 9B) is almost identical to that of the wild type. Insofar as similarity in the

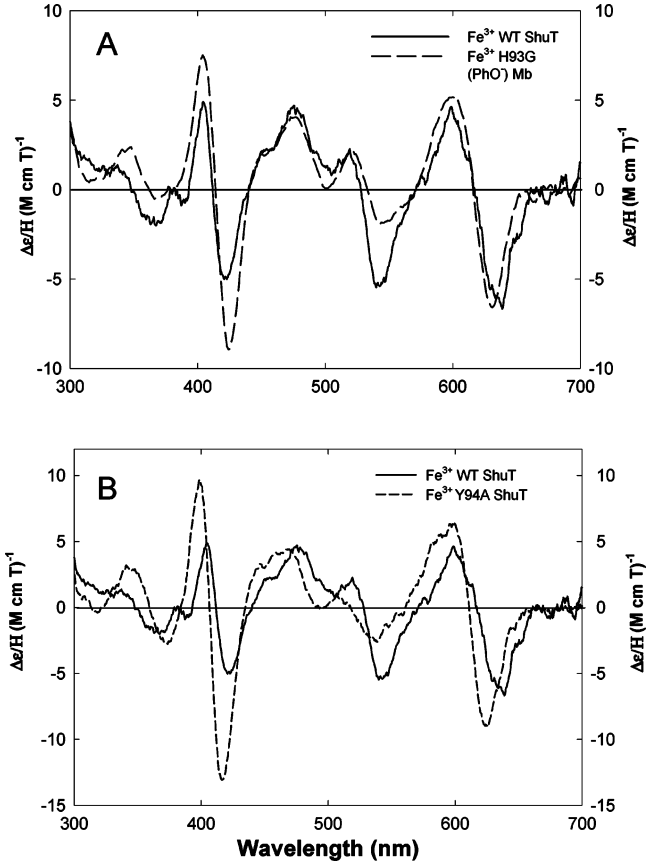

FIGURE 8: Magnetic circular dichroism spectra at 4 °C of (A) ferric wild-type ShuT in 20 mM Tris buffer at pH 7.5 (solid line) and ferric H93G (phenolate/water) myoglobin ([phenol] = 50 mM) in 100 mM potassium phosphate buffer at pH 7.0 (dashed line); (B) Y94A ShuT (dashed line) and wild-type ShuT (solid line).

MCD spectra of Y228F and wild-type ShuT is indicative of similar axial ligand fields, they are consistent with Tyr-228 *not* being the proximal heme ligand. In contrast, there are clear differences between the MCD spectra of ferric WT ShuT and the ShuT(Y94A) and (Y94A/Y228F) mutants in both the visible and Soret regions of the spectrum (Figures 8B and 9A). This contrast in the MCD spectra is consistent with loss of the native proximal ligand, confirming that Y94 is the proximal tyrosine in ferric WT ShuT. Hence, the rR and MCD spectra of WT ShuT and its Tyr mutants are consistent in their support of assigning Tyr-94 as the proximal heme ligand.

The MCD spectra of ferric ShuT(Y94A/Y228F) and alkaline ferric Mb(H93G) are compared in Figure 9C. The latter has been shown to contain a 5C HS-hydroxide complex (*34*). The similarity between these spectra suggests that the double mutant also has a five-coordinate hydroxide ligated structure. Addition of imidazole to the ferric ShuT(Y94A/Y228F) solution yields an imidazole complex whose MCD spectrum (Figure 10) bears a striking resemblance to that of the six-coordinate low-spin imidazole adduct of ferric WT Mb, i.e., a heme with two axial imidazole ligands. The reason for the increased breadth of the Soret feature in the spectrum ShuT(Y94A/Y228F) is not clear, but it may indicate that some heme has dissociated from the protein.

EPR Spectroscopy of WT ShuT. Examination of WT ShuT by X-band EPR spectroscopy at pH 7.0 revealed a rhombic high spin heme having rhombicity of approximately 10%

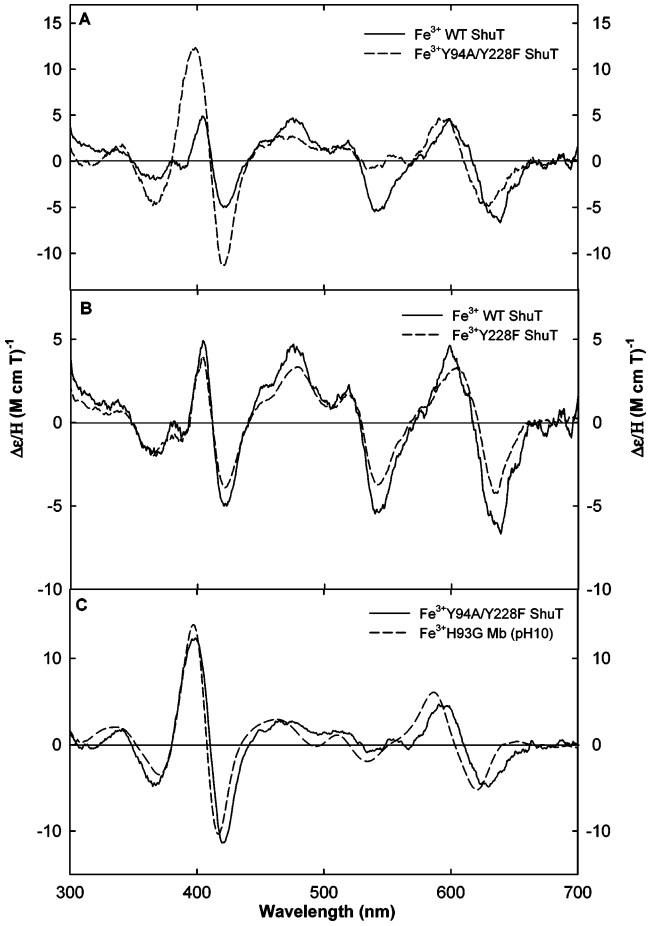

FIGURE 9: Magnetic circular dichroism spectra at 4 °C of (A) ferric wild-type ShuT in 20 mM Tris buffer at pH 7.5 (solid line) and ferric Y94A/Y228F ShuT in 20 mM Tris buffer at pH 7.5 (dashed line); (B) ferric wild-type ShuT in 20 mM Tris buffer at pH 7.5 (solid line) and ferric Y228F ShuT in 20 mM Tris buffer at pH 7.5 (dashed line); (C) ferric Y94A/Y228F ShuT in 20 mM Tris buffer at pH 7.5 (solid line) and ferric H93G (hydroxide) myoglobin in 100 mM potassium phosphate buffer at pH 10.0 (dashed line). The spectrum of ferric H93G (hydroxide) myoglobin is replotted from ref *34*.

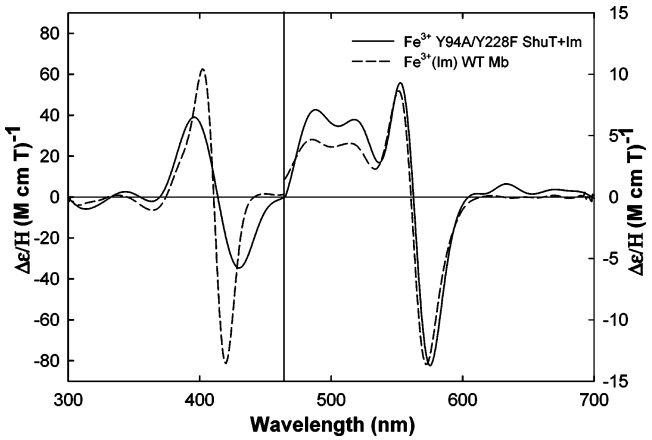

FIGURE 10: Magnetic circular dichroism spectra at 4 °C of ferric Y94A/Y228F ShuT in 20 mM Tris buffer at pH 7.5, 20 mM imidazole (solid line) and the ferric imidazole adduct of wild-type myoglobin in 100 mM potassium phosphate pH 7.0 buffer. The spectrum of ferric imidazole adduct of wild-type myoglobin is replotted from ref *62*.

(Figure S1; Supplementary Information). The *g* values for the specttrum are listed in Table 4. This EPR signature is typical of a ferric high-spin heme having an anionic O-bound axial ligand. This is consistent with the putative ν_{Fe-OPh} mode in the rR spectra of WT ShuT and with the MCD spectrum, as shown in Figures 5 and 9A, respectively.

Table 4: EPR g-Values for Ferric Heme Proteins with Tyrosinate Ligation

protein	g_1	g_2	g_3	ref
WT ShuT	6.29	5.53	1.99	this work
bovine liver catalase	6.60	5.40	2.00	(*60*)
HH Mb(H64Y)	6.64	5.34	1.98	(*61*)
SW Mb(H64Y)	6.63	5.31	1.98	(*35*)

DISCUSSION

Although it is clear that apo-ShuT binds one heme per monomer and that the affinity for heme is high, the ability to quantify the K_d for holo-ShuT is compromised by the propensity of heme to form ill-defined aggregates in aqueous solution (*43*). Moreover, when K_d is in the picomolar to nanomolar range, direct spectrophotometric determination of the fraction bound is challenging at best. While K_d values for the cytoplasmic heme binding protein ShuS from *S. dysenteriae* (*44*) and the rat liver cytosol heme-binding 23 kDa protein (*45*) have been measured directly in the 10^{-6} to 10^{-8} M range by absorbance or fluorescence methods, and K_d for holo-hemopexin has been estimated in the picomolar range (*46*), their absolute thermodynamic stabilities may be of questionable relevance. Although very little physical data are available on the proteins and mechanisms of heme transport, they likely involve interprotein heme transfer mediated by protein−protein interaction, as has been recently demonstrated for metal ion-trafficking systems such as that which facilitates copper transport (*47*). Thus, the first defining aspect of the interactions between heme and its transporters is likely to be high thermodynamic stability, as free heme is toxic. Second, given that heme toxicity requires the affinities of all heme transport proteins to be high, it is likely that their affinities need to be responsive to complexation with the protein that accepts the heme from it. Specifically, the stability of the heme donor protein must be downregulated by the acceptor protein with the energetic cost being paid by the free energy of complexation with the heme acceptor protein.

Even though, in accord with the rR spectra in Figures 4 and 5, the native proximal tyrosinate ligand remains intact in ShuT(Y228F), the rate of heme loss, tracked by its rate of uptake by apo-Mb, is 100 fold greater for ShuT(Y228F) than for the WT protein. This result demonstrates that an increase in the kinetic lability of the heme in holo-ShuT upon replacement of Tyr-228 contributes significantly to the qualitative decrease in affinity for heme. In a complementary fashion, an increase in kinetic lability upon loss of the proximal tyrosinate ligand in the ShuT(Y94A) mutant derives from loss of the coordinative link between the heme and the protein, as revealed by the absence of bands attributable to coordinated tyrosinate in its rR spectrum (Figures 4 and 5).

The optical, vibrational, EPR, and MCD spectral signatures of the heme in ShuT are not atypical of heme proteins having a proximal tyrosinate ligand, such as the eukaryotic (*30*) and bacterial catalase (*31*), the H93Y mutant of myoglobin (*48*, *49*) and the recently characterized sea coral allene oxide

synthase (*50*). Despite the familiarity of this local heme environment, the acquisition and transport of heme into the bacterial cell is likely to require properties atypical of known heme proteins. Specifically, protection of the cell from damage induced by free heme requires proteins having high affinity for heme in its isolated form. On the other hand, both selectivity and kinetic efficacy require that thermodynamic affinities modulated by specific protein−protein interactions between the hemophores and their corresponding heme acceptors. This hypothesis is consistent with the broad pH stability of heme/ShuT observed in this study. We hypothesize that such modulation is affected by specific protein−protein complexes.

The recent structural characterization of the extracellular heme-binding hemophore HasA from *S. marcescens* revealed a novel heme-binding motif in which the heme is held between two loops with His-32 and Tyr-75 providing the ligands to the heme which provides a precedent for a tyrosine histidine ligation in heme-binding proteins involved in heme acquisition (*51*, *52*). While the five-coordinate high spin complex of heme-ShuT is distinct from that of heme-HasA, the hemophore is perhaps the first example of a protein that binds heme with high affinity as it has to displace the heme from hemoglobin, yet it must be capable of releasing the heme to the outer-membrane receptor HasR and therefore sets a precedent for proteins of similar function (*53*). However, sequence homology indicates that the ShuT protein is most closely related to the well-characterized vitamin B_{12} (BtuF) periplasmic binding proteins in which the two-domains are linked by an α-helical segment (Figure 1A) (*15*). The cobalamin cofactor is bound within a deep cleft between the domains of BtuF in the "base-on" conformation wherein the dimethylbenzimidazole (DMB) serves as the axial ligand to the cobalt with six aromatic residues (Tyr-50, Trp-66, Trp-85, Phe-174, Phe-180, and Trp-202), three from each domain with the Trp-65 and Trp-85 side chains flanking the DMB ring. The cobalamin is further stabilized in the binding cleft by a number of hydrogen-bond interactions between amino acid side chains of the corrin ring. Similarly, in the FhuD-hydroxamate siderophore structures the binding site is lined with hydrophobic residues with hydrogen bonding between the hydroxamate and amino acid side chains contributing to the binding affinity (*54*). A recent alignment of the periplasmic proteins that transport siderophores, vitamin B_{12}, and heme based on the structure of the FhuD−hydroxamate complexes suggests that they belong to a distinct family of periplasmic binding proteins, in which many of the conserved residues including those lining the binding pocket are retained (*13*). Sequence alignment of BtuF and ShuT indicates that conserved aromatic residues that are directly involved in cobalamin binding in BtuF, specifically, Trp-66 and Trp-85, are conserved, corresponding to Trp-95 and Trp-114 in ShuT (*15*). Consistent with these sequence identities, recently obtained electron density maps of ShuT indicate a number of hydrophobic residues lining the heme-binding cleft supporting the conserved nature of this family of periplasmic binding proteins (Lanzilotta, W., personal communication).

The crystal structures of the apo and substrate bound BtuF suggest that local unwinding of the α-helix connecting the two domains is responsible for the increased mobility in the apo-form, while binding of cobalamin reduces the flexibility in the holoprotein (*21*). The mechanism of transport is proposed to involve conformational change driven by the protein−protein interaction at the domain interface between the PBP and the ABC transporter and an ATP-driven conformational change or "tweezer" motion that promotes release of substrate to the cytoplasm (*15*, *23*). A model for docking of BtuF with its cognizant ABC transporter BtuCD is thought to involve a conserved Glu residue at the surface of each domain (Glu-72 and Glu-202) of BtuF with a complementary set of conserved Arg residues in BtuCD (*15*). Interestingly, the regions containing the conserved Glu residues are present in ShuT corresponding to residues Glu-101 and Glu-234, respectively, suggesting a conserved mechanism for docking of the carrier protein to the periplasmic domain of the receptor (Figure 1A). On interaction of the soluble periplasmic receptor with the ABC transporter a sequence of events is thought to occur in which a conformational change induced by the protein−protein interaction releases the heme, after which a tweezer-like motion driven by ATP hydrolysis in the ATPase domain induces release of the heme to the cytoplasm (*22*). Although the conformational changes undertaken by the PBPs such as the leucine-binding protein are quite large hinge and twist motions, the vitamin B_{12} (BtuF) and iron-hydroxamate (FhuD) proteins are not expected to undergo such drastic changes (*15*). However, in the Zn-binding protein TroA from *Treponema pallidum* (a structural homologue of BtuF) differences between the unliganded (*55*) and the liganded (*56*) protein indicate a four degree tilting between the domains, which is sufficient to disrupt the Zn-binding site. Thus, it is possible that ShuT, which falls within this family of periplasmic binding proteins, may undergo similar domain tilting that brings about changes in coordination sufficient to promote release of the heme to the ABC transporter.

In summary, we present the first characterization of a periplasmic heme-binding protein to which the heme is 5C HS with Tyr-94 providing the proximal ligand to the heme. Additionally, a number of H-bonding and hydrophobic interactions most likely contribute to the high-affinity binding. The insensitivity of heme−ShuT spectroscopic signatures to pH, together with the relative redox inactivity suggests that the protein has evolved to complex the heme with high affinity, the release of which is triggered by interaction with the cytoplasmic ABC transporter. Studies on the interplay between heme coordination, conformational changes, interaction with the ABC transporter, and heme release are currently underway.

ACKNOWLEDGMENT

A.W. would like to thank Shelley Payne for the gift of the pSHU262 plasmid and Kimberly Burkhard, Mario Rivera, and Bill Lanzilotta for helpful discussions. J.H.D. and S.S. would like to especially thank Roshan Perera for the MCD spectrum of ferric H93G (phenolate/water) myoglobin. The authors would like to thank Prof. W. Robert Scheidt for access to EPR facilities and Dr. Graeme Wyllie for recording the EPR spectra.

REFERENCES

1. Henderson, D. P., and Payne, S. M. (1993) Cloning and characterization of the *Vibrio cholerae* genes encoding the utilization of iron from haemin and haemoglobin. *Mol. Microbiol. 7*, 461−469.

2. Hornung, J. M., Jones, H. A., and Perry, R. D. (1996) The hmu locus of *Yersinia pestis* is essential for utilization of free haemin and haem−protein complexes as iron sources. *Mol. Microbiol. 20*, 725−739.
3. Mills, M., and Payne, S. M. (1995) Genetics and regulation of heme iron transport in *Shigella dysenteriae* and detection of an analogous system in *Escherichia coli* O157: H7. *J. Bacteriol. 177*, 3004−3009.
4. Stojiljkovic, I., and Hantke, K. (1992) Hemin uptake system of *Yersinia enterocolitica*: similarities with other TonB-dependent systems in gram-negative bacteria. *EMBO J. 11*, 4359−4367.
5. Wyckoff, E. E., Duncan, D., Torres, A. G., Mills, M., Maase, K., and Payne, S. M. (1998) Structure of the *Shigella dysenteriae* haem transport locus and its phylogenetic distribution in enteric bacteria. *Mol. Microbiol. 28*, 1139−1152.
6. Braun, V. (2001) Iron uptake mechanisms and their regulation in pathogenic bacteria. *Int. J. Med. Microbiol. 291*, 67−79.
7. Braun, V., and Braun, M. (2002) Iron transport and signaling in *Escherichia coli*. *FEBS Lett. 529*, 78−85.
8. Brown, J. S., and Holden, D. W. (2002) Iron acquisition by Gram-positive bacterial pathogens. *Microbes Infect. 4*, 1149−1156.
9. Clarke, T. E., Tari, L. W., and Vogel, H. J. (2001) Structural biology of bacterial iron uptake systems. *Curr. Top. Med. Chem. 1*, 7−30.
10. Mills, M., and Payne, S. M. (1997) Identification of *shuA*, the gene encoding the heme receptor of *Shigella dysenteriae*, and analysis of invasion and intracellular multiplication of a shuA mutant. *Infect. Immun. 65*, 5358−5363.
11. Sprencel, C., Cao, Z., Qi, Z., Scott, D. C., Montague, M. A., Ivanoff, N., Xu, J., Raymond, K. M., Newton, S. M., and Klebba, P. E. (2000) Binding of ferric enterobactin by the *Escherichia coli* periplasmic protein FepB. *J. Bacteriol. 182*, 5359−5364.
12. Stephens, D. L., Choe, M. D., and Earhart, C. F. (1995) *Escherichia coli* periplasmic protein FepB binds ferrienterobactin. *Microbiology 141*, 1647−1654.
13. Clarke, T. E., Rohrbach, M. R., Tari, L. W., Vogel, H. J., and Koster, W. (2002) Ferric hydroxamate binding protein FhuD from *Escherichia coli*: mutants in conserved and nonconserved regions. *Biometals 15*, 121−131.
14. Koster, W., and Braun, V. (1989) Iron-hydroxamate transport into *Escherichia coli* K12: localization of FhuD in the periplasm and of FhuB in the cytoplasmic membrane. *Mol. Gen. Genet. 217*, 233−239.
15. Borths, E. L., Locher, K. P., Lee, A. T., and Rees, D. C. (2002) The structure of *Escherichia coli* BtuF and binding to its cognate ATP binding cassette transporter. *Proc. Natl. Acad. Sci. U.S.A. 99*, 16642−16647.
16. Higgins, C. F. (2001) ABC transporters: physiology, structure and mechanism−an overview. *Res. Microbiol. 152*, 205−210.
17. Linton, K. J., and Higgins, C. F. (1998) The *Escherichia coli* ATP-binding cassette (ABC) proteins. *Mol. Microbiol. 28*, 5−13.
18. Shea, C. M., and McIntosh, M. A. (1991) Nucleotide sequence and genetic organization of the ferric enterobactin transport system: homology to other periplasmic binding protein-dependent systems in *Escherichia coli*. *Mol. Microbiol. 5*, 1415−1428.
19. Davidson, A. L. (2002) Mechanism of coupling of transport to hydrolysis in bacterial ATP-binding cassette transporters. *J. Bacteriol. 184*, 1225−1233.
20. Quiocho, F. A., and Ledvina, P. S. (1996) Atomic structure and specificity of bacterial periplasmic receptors for active transport and chemotaxis: variation of common themes. *Mol. Microbiol. 20*, 17−25.
21. Karpowich, N. K., Huang, H. H., Smith, P. C., and Hunt, J. F. (2003) Crystal structures of the BtuF periplasmic-binding protein for vitamin B12 suggest a functionally important reduction in protein mobility upon ligand binding. *J. Biol. Chem. 278*, 8429−8434.
22. Chen, J., Lu, G., Lin, J., Davidson, A. L., and Quiocho, F. A. (2003) A tweezers-like motion of the ATP-binding cassette dimer in an ABC transport cycle. *Mol. Cell 12*, 651−661.
23. Chen, J., Sharma, S., Quiocho, F. A., and Davidson, A. L. (2001) Trapping the transition state of an ATP-binding cassette transporter: evidence for a concerted mechanism of maltose transport. *Proc. Natl. Acad. Sci. U.S.A. 98*, 1525−1530.
24. Quiocho, F. A. (1990) Atomic structures of periplasmic binding proteins and the high-affinity active transport systems in bacteria. *Philos. Trans. R. Soc. Lond. B Biol. Sci. 326*, 341−351; discussion 351−352.
25. Sambrook, J., Fritsch, E. F., and Maniatis, T. (1989) *Molecular Cloning: A Laboratory Manual*, Cold Spring Harbor Laboraory, Cold Spring Harbor, NY.
26. Huff, A. M., Chang, C. K., Cooper, D. K., Smith, K. M., and Dawson, J. H. (1993) Imidazole- and Alkylamine-Ligated Iron (II, III) Chlorin Complexes as Models for Histidine and Lysine Coordination to the Iron in Dihydroporphyrin-Containing Proteins: Characterization with Magnetic Circular Dichroism Spectroscopy. *Inorg. Chem. 32*, 1460−1466.
27. Perera, R., and Dawson, J. H. (2004) Modelling Heme Protein Active Sites with the His93Gly Cavity Mutant of Sperm Whale Myoglobin: Complexes with Nitrogen-, Oxygen-, and Sulfur-Donor Proximal Ligands. *J. Porphyrins Phthalocyanines 8*, 246−254.
28. Nielsen, H., Engelbrecht, J., Brunak, S., and von Heijne, G. (1997) Identification of prokaryotic and eukaryotic signal peptides and prediction of their cleavage sites. *Protein Eng. 10*, 1−6.
29. Jin, Y., Nagai, M., Nagai, Y., Nagatomo, S., and Kitagawa, T. (2004) Heme structures of five variants of hemoglobin M probed by resonance Raman spectroscopy. *Biochemistry 43*, 8517−8527.
30. Reid, T. J., 3rd, Murthy, M. R., Sicignano, A., Tanaka, N., Musick, W. D., and Rossmann, M. G. (1981) Structure and heme environment of beef liver catalase at 2.5 A resolution. *Proc. Natl. Acad. Sci. U.S.A. 78*, 4767−4771.
31. Sharma, K. D., Andersson, L. A., Loehr, T. M., Terner, J., and Goff, H. M. (1989) Comparative spectral analysis of mammalian, fungal, and bacterial catalases. Resonance Raman evidence for iron-tyrosinate coordination. *J. Biol. Chem. 264*, 12772−12779.
32. Liu, Y., Moënne-Loccoz, P., Hildebrand, D. P., Wilks, A., Loehr, T. M., Mauk, A. G., and Ortiz de Montellano, P. R. (1999) Replacement of the Proximal Histidine Iron Ligand by a Cysteine or Tyrosine Converts Heme Oxygenase to an Oxidase. *Biochemistry 38*, 3733−3743.
33. Sun, J., Loehr, T. M., Wilks, A., and Ortiz de Montellano, P. R. (1994) Identification of histidine 25 as the heme ligand in human liver heme oxygenase. *Biochemistry 33*, 13734−13740.
34. Pond, A. E., Roach, M. P., Sono, M., Rux, A. H., Franzen, S., Hu, R., Thomas, M. R., Wilks, A., Dou, Y., Ikeda-Saito, M., Ortiz de Montellano, P. R., Woodruff, W. H., Boxer, S. G., and Dawson, J. H. (1999) Assignment of the Heme Axial Ligand(s) for the Ferric Myoglobin (H93G) and Heme Oxygenase (H25A) Cavity Mutants as Oxygen Donors Using Magnetic Circular Dichroism. *Biochemistry 38*, 7601−7608.
35. Egeberg, K. D., Springer, B. A., Martinis, S. A., Sligar, S. G., Morikis, D., and Champion, P. M. (1990) Alteration of sperm whale myoglobin heme axial ligation by site-directed mutagenesis. *Biochemistry 29*, 9783−9791.
36. Uchida, T., Stevens, J. M., Daltrop, O., Harvat, E. M., Hong, L., Ferguson, S. J., and Kitagawa, T. (2004) The interaction of covalently bound heme with the cytochrome *c* maturation protein CcmE. *J. Biol. Chem. 279*, 51981−51988.
37. Das, T. K., Franzen, S., Pond, A., Dawson, J. H., and Rousseau, D. L. (1999) Formation of a Five-Coordinate Hydroxide-Bound Heme in the His93Gly Mutant of Sperm Whale Myoglobin. *Inorg. Chem. 38*, 1952−1953.
38. Das, T. K., Boffi, A., Chiancone, E., and Rousseau, D. L. (1999) Hydroxide rather than histidine is coordinated to the heme in five-coordinate ferric *Scapharca inaequivalvis* hemoglobin. *J. Biol. Chem. 274*, 2916−2919.
39. Chu, G. C., Couture, M., Yoshida, T., Rousseau, D. L., and Ikeda-Saito, M. (2000) Axial ligation states of five-coordinate heme oxygenase proximal histidine mutants, as revealed by EPR and resonance Raman spectroscopy. *J. Am. Chem. Soc. 122*, 12612−12613.
40. Boffi, A., Das, T. K., della Longa, S., Spagnuolo, C., and Rousseau, D. L. (1999) Pentacoordinate hemin derivatives in sodium dodecyl sulfate micelles: model systems for the assignment of the fifth ligand in ferric heme proteins. *Biophys. J. 77*, 1143−1149.
41. Reed, R. A., Rodgers, K. R., Kushmeider, K., Spiro, T. G., and Su, Y. O. (1990) Iron-Hydroxide Stretching Resonance Raman Bands of a Water-Soluble Sterically Hindered Porphyrin. *Inorg. Chem. 29*, 2881−2883.
42. Chuang, W. J., Johnson, S., and Van Wart, H. E. (1988) Resonance Raman spectra of bovine liver catalase: enhancement of proximal tyrosinate vibrations. *J. Inorg. Biochem. 34*, 201−219.
43. Kuzelova, K., Mrhalova, M., and Hrkal, Z. (1997) Kinetics of heme interaction with heme-binding proteins: the effect of heme aggregation state. *Biochim. Biophys. Acta 1336*, 497−501.

44. Wilks, A. (2001) The ShuS protein of *Shigella dysenteriae* is a heme-sequestering protein that also binds DNA. *Arch. Biochem. Biophys. 387*, 137−142.
45. Iwahara, S., Satoh, H., Song, D. X., Webb, J., Burlingame, A. L., Nagae, Y., and Muller-Eberhard, U. (1995) Purification, characterization, and cloning of a heme-binding protein (23 kDa) in rat liver cytosol. *Biochemistry 34*, 13398−13406.
46. Hrkal, Z., Vodrazka, Z., and Kalousek, I. (1974) Transfer of heme from ferrihemoglobin and ferrihemoglobin isolated chains to hemopexin. *Eur. J. Biochem. 43*, 73−78.
47. Huffman, D. L., and O'Halloran, T. V. (2001) Function, structure, and mechanism of intracellular copper trafficking proteins. *Annu. Rev. Biochem. 70*, 677−701.
48. Adachi, S., Nagano, S., Ishimori, K., Watanabe, Y., Morishima, I., Egawa, T., Kitagawa, T., and Makino, R. (1993) Roles of proximal ligand in heme proteins: replacement of proximal histidine of human myoglobin with cysteine and tyrosine by site-directed mutagenesis as models for P-450, chloroperoxidase, and catalase. *Biochemistry 32*, 241−252.
49. Hildebrand, D. P., Burk, D. L., Maurus, R., Ferrer, J. C., Brayer, G. D., and Mauk, A. G. (1995) The proximal ligand variant His93Tyr of horse heart myoglobin. *Biochemistry 34*, 1997−2005.
50. Abraham, B. D., Sono, M., Boutaud, O., Shriner, A., Dawson, J. H., Brash, A. R., and Gaffney, B. J. (2001) Characterization of the coral allene oxide synthase active site with UV−visible absorption, magnetic circular dichroism, and electron paramagnetic resonance spectroscopy: evidence for tyrosinate ligation to the ferric enzyme heme iron. *Biochemistry 40*, 2251−2259.
51. Arnoux, P., Haser, R., Izadi, N., Lecroisey, A., Delepierre, M., Wandersman, C., and Czjzek, M. (1999) The crystal structure of HasA, a hemophore secreted by *Serratia marcescens*. *Nat. Struct. Biol. 6*, 516−520.
52. Arnoux, P., Haser, R., Izadi-Pruneyre, N., Lecroisey, A., and Czjzek, M. (2000) Functional aspects of the heme bound hemophore HasA by structural analysis of various crystal forms. *Proteins 41*, 202−210.
53. Izadi, N., Henry, Y., Haladjian, J., Goldberg, M. E., Wandersman, C., Delepierre, M., and Lecroisey, A. (1997) Purification and characterization of an extracellular heme-binding protein, HasA, involved in heme iron acquisition. *Biochemistry 36*, 7050−7057.
54. Clarke, T. E., Braun, V., Winkelmann, G., Tari, L. W., and Vogel, H. J. (2002) X-ray crystallographic structures of the *Escherichia coli* periplasmic protein FhuD bound to hydroxamate-type siderophores and the antibiotic albomycin. *J. Biol. Chem. 277*, 13966−13972.
55. Lee, Y. H., Dorwart, M. R., Hazlett, K. R., Deka, R. K., Norgard, M. V., Radolf, J. D., and Hasemann, C. A. (2002) The crystal structure of Zn(II)-free *Treponema pallidum* TroA, a periplasmic metal-binding protein, reveals a closed conformation. *J. Bacteriol. 184*, 2300−2304.
56. Lee, Y. H., Deka, R. K., Norgard, M. V., Radolf, J. D., and Hasemann, C. A. (1999) *Treponema pallidum* TroA is a periplasmic zinc-binding protein with a helical backbone. *Nat. Struct. Biol. 6*, 628−633.
57. Das, T. K., Couture, M., Lee, H. C., Peisach, J., Rousseau, D. L., Wittenberg, B. A., Wittenberg, J. B., and Guertin, M. (1999) Identification of the ligands to the ferric heme of *Chlamydomonas* chloroplast hemoglobin: evidence for ligation of tyrosine-63 (B10) to the heme. *Biochemistry 38*, 15360−15368.
58. Nagai, K., Kagimoto, T., Hayashi, A., Taketa, F., and Kitagawa, T. (1983) Resonance Raman studies of hemoglobins M: evidence for iron-tyrosine charge-transfer interactions in the abnormal subunits of Hb M Boston and Hb M Iwate. *Biochemistry 22*, 1305−1311.
59. Nagai, M., Yoneyama, Y., and Kitagawa, T. (1989) Characteristics in tyrosine coordinations of four hemoglobins M probed by resonance Raman spectroscopy. *Biochemistry 28*, 2418−2422.
60. Deisseroth, A., and Dounce, A. L. (1970) Catalase: Physical and chemical properties, mechanism of catalysis, and physiological role. *Physiol. Rev. 50*, 319−375.
61. Maurus, R., Bogumil, R., Luo, Y., Tang, H. L., Smith, M., Mauk, A. G., and Brayer, G. D. (1994) Structural characterization of heme ligation in the His64 → Tyr variant of myoglobin. *J. Biol. Chem. 269*, 12606−12610.
62. Pond, A. E., Roach, M. P., Thomas, M. R., Boxer, S. G., and Dawson, J. H. (2000) The H93G myoglobin cavity mutant as a versatile template for modeling heme proteins: ferrous, ferric, and ferryl mixed-ligand complexes with imidazole in the cavity. *Inorg. Chem. 39*, 6061−6066.

BI050422R